Experimental and Quantum Chemical Study of the Mechanism of an Unexpected Intramolecular Reductive Coupling of a Bridging Phosphido Ligand and a C_6F_5 Group and the Reversible Oxidative Addition of $PPh_2C_6F_5$[#,||]

Naima Chaouche,[†,‡] Juan Forniés,*[,†] Consuelo Fortuño,[†] Abdelaziz Kribii,[‡] Antonio Martín,[†] Paraskevas Karipidis,[§] Athanassios C. Tsipis,[⊥] and Constantinos A. Tsipis*[,§]

Departamento de Química Inorgánica and Instituto de Ciencia de Materiales de Aragón, Universidad de Zaragoza−CSIC, 50009 Zaragoza, Spain, Département de Chimie, Faculté des Sciences, Université IbnTofail, B. P. 133, Kenitra, Morocco, Laboratory of Applied Quantum Chemistry, Faculty of Chemistry, Aristotle University of Thessaloniki, 541 24 Thessaloniki, Greece, and Laboratory of Inorganic Chemistry, Department of Chemistry, University of Ioannina, 451 10 Ioannina, Greece

Received October 15, 2003

Downloaded by NAT LIB UKRAINE on July 4, 2009
Published on March 18, 2004 on http://pubs.acs.org | doi: 10.1021/om034236y

The two-electron oxidation reactions of the $[NBu_4]_2[(C_6F_5)_2M(\mu\text{-}PPh_2)_2M'(C_6F_5)_2]$ (M = M′ = Pt, **1a**; M = M′ = Pd, **1b**; M = Pt, M′ = Pd, **1c**) complexes using I_2 as oxidant have been investigated by experimental and electronic structure calculation methods. The geometric and energetic reaction profiles in a vacuum have been investigated at the B3LYP/LANL2DZ level. The first step of the oxidation processes involves the oxidative addition of I_2 to one of the four-coordinate M(II) metal centers yielding a five-coordinate intermediate with square pyramidal stereochemistry. The oxidized $[(I)L_2M(\mu\text{-}PH_2)_2M'L_2]^-$ (L = CN) complex converts to a more stable intermediate involving a planar dimetallacycle five-membered ring, which through a reactant-like transition state surmounting a relatively low barrier of 18.5, 8.7, and 8.9 kcal/mol for Pt_2, PtPd, and Pd_2 compounds, respectively, yields the final product. At this stage an unusual intramolecular reductive coupling of one of the ancillary ligands with a bridging phosphido ligand takes place, affording the "M(II)(μ-PH_2)(μ-I)M′(II)" framework. This process is exoergic by 11.4, 18.2, and 18.8 kcal/mol for Pt_2, PtPd, and Pd_2 compounds, respectively. For the Pt_2 and PtPd complexes removal of the iodide ligand from the oxidized iodo complexes yields the very unusual $[L_2M^{III}(\mu\text{-}PH_2)_2M'^{III}L_2]$ (L = CN or C_6F_5) complexes. In contrast, $[L_2Pd^{III}(\mu\text{-}PH_2)_2Pd^{III}L_2]$ does not exist as local minima in the PES, but the $[L_2Pd^{II}(\mu\text{-}PH_2)Pd^{II}(PH_2L)L]$ species was identified, resulting from the intramolecular reductive coupling promoted by the iodide ligand abstraction. This species could be considered as an intermediate for the reverse intramolecular oxidative addition of the PH_2L ligand promoted by iodide abstraction with Ag^+ ions. Finally, the molecular structure of the $[(C_6F_5)_2Pt(\mu\text{-}PPh_2)(\mu\text{-}I)Pd(C_6F_5)\{PPh_2(C_6F_5)\}]$ complex has been established by X-ray crystallography.

Introduction

The ability of the anionic perhalophenylplatinate complexes to act as Lewis bases affording polynuclear complexes with Pt→M donor−acceptor bonds is well documented[1,2] (see Scheme 1a).

In the course of our current research interests on transition metal diphenylphosphido complexes we decided several years ago to study the reaction of the $[NBu_4]_2[(C_6F_5)_2M(\mu\text{-}PPh_2)_2M'(C_6F_5)_2]$ (M = M′ = Pt, **1a**; M = M′ = Pd, **1b**; M = Pt, M′ = Pd, **1c**) complexes with $AgClO_4$, aiming to prepare polynuclear complexes of silver coordinated with the platinate fragment acting as chelating bidentate ligand (see Scheme 1b).

To our surprise, the reaction of **1a** did not afford the expected trinuclear Pt_2Ag derivative, but the binuclear Pt(III)−Pt(III) complex formulated as $[(C_6F_5)_2Pt(\mu\text{-}PPh_2)_2Pt(C_6F_5)_2]$, **2**, was isolated through an oxidation process with the Ag^+ ions acting as the oxidant[3]

[#] Dedicated to Professor José Vicente (Universidad de Murcia) on the occasion of his 60th birthday.

[||] Polynuclear Homo- or Heterometallic Palladium(II)−Platinum(II) Pentafluorophenyl Complexes Containing Bridging Diphenylphosphido Ligands. 14. For part 13 see ref 58.

* Corresponding authors. E-mail: forniesj@unizar.es (J.F.). Tel: (+2310) 997851. Fax: (+2310) 997851. E-mail: tsipis@chem.auth.gr (C.A.T.).

[†] Universidad de Zaragoza−CSIC.

[‡] Université IbnTofail.

[§] Aristotle University of Thessaloniki.

[⊥] University of Ioannina.

(1) Forniés, J.; Martín, A. In *Metal Clusters in Chemistry*; Braunstein, P., Oro, L. A., Raithby, P. R., Eds.; Wiley-VCH: Weinheim (Germany), 1999; Vol. 1, pp 417−443.

(2) Usón, R.; Forniés, J. *Inorg. Chim. Acta* **1992**, *200*, 165−177.

(3) Alonso, E.; Casas, J. M.; Cotton, F. A.; Feng, X. J.; Forniés, J.; Fortuño, C.; Tomás, M. *Inorg. Chem.* **1999**, *38*, 5034−5040.

10.1021/om034236y CCC: $27.50 © 2004 American Chemical Society
Publication on Web 03/18/2004

Scheme 1

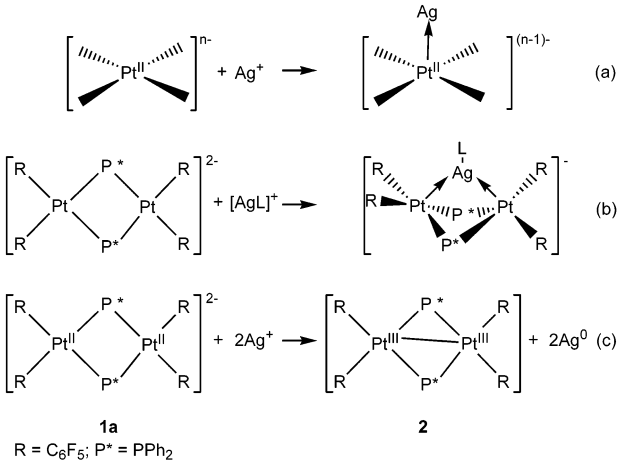

(see Scheme 1c). However, reacting the analogues **1b** and **1c** with $AgClO_4$, under similar conditions, no analogous M(III)−M′(III) derivatives ($[(C_6F_5)_2M(\mu\text{-}PPh_2)_2M'(C_6F_5)_2]$ (M = M′ = Pd, **2b**; M = Pd, M′ = Pt, **2c**) could be isolated, since decomposition of the resulting solutions occurs, yielding dark mixtures from which the aforementioned complexes were impossible to be separated and identified. Complex **2** is very unusual because it displays the platinum centers in square planar coordination environments involving a coplanar Pt(III)−Pt(III) bond (see Scheme 1c). On the other hand, complexes **1a**, **1b**, and **1c** exhibit a quite similar electrochemical behavior.[3] With this in mind we thought it would be advisable to study their oxidation reactions using I_2 as an oxidant, aiming to obtain homo- or heterobinuclear complexes with the metal centers in formal oxidation state higher than 2, the stability of the bridging system "$M(\mu\text{-}PPh_2)_2M'$" maintaining the integrity of the binuclear fragment.

Here we report on the results of a detailed experimental and quantum chemical study of the peculiar behavior of the $[NBu_4]_2[(C_6F_5)_2M(\mu\text{-}PPh_2)_2M'(C_6F_5)_2]$ (M = M′ = Pt, **1a**; M = M′ = Pd, **1b**; M = Pt, M′ = Pd, **1c**) complexes toward the oxidation with iodine, a complex process accompanied by an unexpected intramolecular reductive coupling followed by a reversible oxidative addition reaction. Electronic structure calculations based on density functional theory (DFT) methods threw light on the mechanism of the respective reactions in a vacuum, identifying possible reaction pathways and providing both the geometric and energetic profile of the reactions.

Results and Discussion

1. Synthesis. The addition of I_2 to a colorless solution of **1a** in CH_2Cl_2 (1:1 molar ratio) at 195 K renders instantaneously a yellow solution, from which the binuclear Pt(III) complex **2** is isolated (75% yield) (Scheme 2a). It is well known that oxidative addition of X_2 (X = halogen) to Pd(II) and Pt(II) complexes affords by a 2*e* oxidation process halo-M(IV) complexes. Surprisingly, the reaction of **1a** with I_2 (1:1 molar ratio) at 195 K follows a different pathway involving elimination of the I^- ligands from the platinum centers, thus affording the neutral binuclear Pt(III) complex $[(C_6F_5)_2\text{-}Pt(\mu\text{-}PPh_2)_2Pt(C_6F_5)_2]$, **2**, in high yield. On the other hand, treatment of **1b** or **1c** with I_2 (1:1 molar ratio) at 195 K does not render, as expected, the analogous Pt(III)−Pd(III) or Pd(III)−Pd(III) complexes, but the binuclear derivatives formulated as $[NBu_4][(C_6F_5)_2M(\mu\text{-}PPh_2)(\mu\text{-}I)M'(C_6F_5)(PPh_2C_6F_5)]$ (M = M′ = Pd, **3b**; M = Pt, M′ = Pd, **3c**) are isolated as yellow solids (Scheme 2b).

Scheme 2

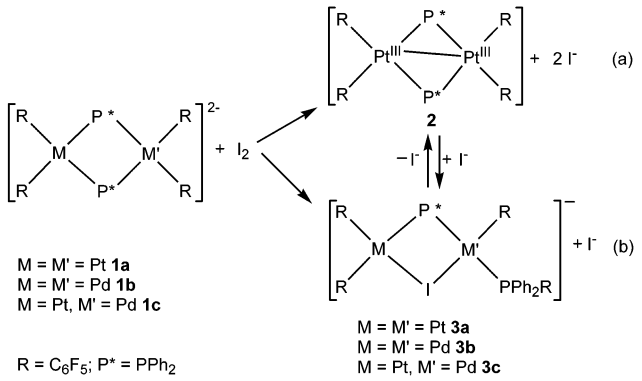

Aiming to throw some light on these electron transfer processes, we have added I_2 to CD_2Cl_2 solutions of **1a** and **1c** (1:1 molar ratio) at 213 K and monitored the processes by ^{19}F NMR spectroscopy. In the first case of the diplatinum species (Pt_2), the colorless solution of **1a** becomes yellow upon addition of I_2 and the spectrum at 213 K shows only signals due to complex **2**. By increasing the temperature in 10-deg intervals up to 313 K, it can be observed that additional signals emerge at 263 K, with a concomitant decrease of the intensity of the signals assigned to **2**. At the end, only the signals due to $[NBu_4][(C_6F_5)_2Pt(\mu\text{-}PPh_2)(\mu\text{-}I)Pt(C_6F_5)(PPh_2C_6F_5)]$, **3a**, are observed and the solution turns colorless. Nevertheless, for **1c** the spectrum at 213 K already exhibits a large number of very broad and overlapping signals, while at 293 K the pattern of the spectrum is that observed for **3c**. Because of the complexity of the NMR spectra, no information with respect to intermediate species present at low temperature can be obtained. Typically, the reaction of **1a** involves an oxidative addition of the I_2 molecule to the platinum centers followed by the elimination of iodide ligands, which results in the formation of the neutral binuclear Pt(III) complex **2**, without changing the "$Pt(\mu\text{-}PPh_2)_2Pt$" framework. It is worth noting that at 213 K the only species detected is **2**. However, in the presence of iodide anions and at higher temperatures complex **2** is not stable enough, and it is immediately transformed to **3a** through the reductive coupling of a phosphido ligand with a pentafluorophenyl group, affording a coordinated tertiary phosphane ($PPh_2C_6F_5$) ligand. In **3a** the Pt(II) coordination spheres are completed by the iodide ligand, thus giving rise to the "$Pt(II)(\mu\text{-}PPh_2)(\mu\text{-}I)Pt(II)$" framework (see Scheme 2b). When the binuclear starting material contains at least one palladium center, the elusive Pt and/or Pd(III) complexes **2b**,**c**, if formed, could not be detected, even at low temperature, indicating that the reductive coupling of the phosphido and pentafluorophenyl groups takes place very fast.

When the yellow solution of **2** is stirred at room temperature in the presence of iodide anions, the color fades, and after stirring for 20 h a colorless solution

Downloaded by NAT LIB UKRAINE on July 4, 2009
Published on March 18, 2004 on http://pubs.acs.org | doi: 10.1021/om034236y

Downloaded by NAT LIB UKRAINE on July 4, 2009
Published on March 18, 2004 on http://pubs.acs.org | doi: 10.1021/om034236y

results, in line with the NMR information. From this solution **3a** is isolated as a white solid.

The ^{19}F NMR spectra of **3a**−**c** registered in deuteroacetone show in the usual region of *o*-F atoms of the C_6F_5 groups bonded to the metal centers three signals (intensity ratio 2:2:2) with the expected platinum satellites. In the usual region of *p*- and *m*-F atoms of the C_6F_5 groups bonded to the metals appear the expected six signals (intensity ratio 1:1:2:2:2:1) for **3a**. For **3b**,**c** two of these signals appear overlapped, giving rise to five signals in the intensity ratio 1:2:1:3:2 and 1:2:1:2:3, respectively (see Experimental Section). All these data are in agreement with the inequivalence of the three C_6F_5 groups bonded to platinum and/or palladium centers and with the equivalence of both halves of each C_6F_5 ring. Moreover, the spectra show signals due to another type of C_6F_5 group. The ones due to *o*-F (−124.5 (**3a**), −124.3 (**3b**), and −124.4 (**3c**) ppm and intensity ratio of 2) and *p*-F (−152.0 (**3a**), −151.9 (**3b**), and −152.0 (**3c**) ppm and intensity ratio of 1) appear in a striking region, while the signals due to *m*-F (−162.9 (**3a**), −162.5 (**3b** and **3c**) ppm and intensity ratio of 2) appear only slightly lower field than the *m*-F and *p*-F signals of the other C_6F_5 groups. These signals can be assigned unequivocally to the phosphane pentafluorophenyl ring. These upfield and downfield changes in the chemical shifts of *o*-F and *p*-F signals, respectively, have been observed in pentafluorophenyl organic ligands.[4−7] The $^{31}P\{^1H\}$ NMR spectra of **3a**−**c** show two doublets (AX spin system) for **3a** and **3c**. For **3b** the pattern must be analyzed as an AB spin system. In all cases the signal that appears to more upfield is broad, as is usual in all our diphenylphosphido derivatives with C_6F_5 groups in *trans* position.[8,9] Moreover, in complex **3a** this signal shows platinum satellites from which two values of $^1J_{Pt-P}$ can be extracted, and in complex **3c** only this signal shows platinum satellites (see Experimental Section). From all these data the unambiguous assignment of this signal to the P atom of the PPh_2 ligand can be made. We have extensively observed that the chemical shifts of P atoms in bridged phosphido derivatives can be very informative not only if the metal atoms are joined or not by metal−metal bond but if a single or two PPh_2 groups are bridging the metal centers.[4,8,10] In agreement with this, the chemical shifts of the PPh_2 ligand in **3a**−**c** (from 4 to −55 ppm) appear at lower field that those of the $M(\mu\text{-}PPh_2)_2M'$ framework in the starting materials (from −106 to −147 ppm) and are in the same range as those observed for other derivatives that show the $M(\mu\text{-}PPh_2)(\mu\text{-}X)M'$ (X = Cl, Br, OH) framework without metal−metal bond.[11,12] It has been established that usually the chemical shift decreases as the atomic number increases from top to bottom in a triad.[13] In agreement with this the chemical shifts from **3b** (Pd_2, 3.9 ppm) to **3c** (PdPt, −18.7 ppm) and to **3a** (Pt_2, −55.3 ppm) show that this P atom is shielded upon substitution of a palladium by a platinum center, as observed previously.[14]

The ^1H NMR spectra of **3a**−**c** have been recorded in deuteroacetone and show signals due to phenylic H atoms and those expected for the NBu_4^+. The intensity of these signals is in agreement with the monoanionic nature of the complexes.

In the IR spectra of **3b**,**c**, the X-sensitive modes of the C_6F_5 groups appear as one strong and one (**3a**,**b**) or two (**3c**) medium absorptions (see Experimental Section). Besides the strong signals around 1500 and 950 cm^{-1} always observed in all pentafluorophenyl derivatives with an $M-C_6F_5$ bond, two other absorptions at higher frequencies, ca. 1520 and 980 cm^{-1}, are observed at these regions in complexes **3a**−**c**. Analogous absorptions have been observed for two other complexes prepared by us some years ago, $[Pt_2Pd_2(\mu\text{-}PPh_2)_3(C_6F_5)_3(PPh_2C_6F_5)(CO)]$ and $[Pt_2Pd_2(\mu\text{-}PPh_2)_3(C_6F_5)_3(PPh_2C_6F_5)]$.[4] Thus we can now establish that the presence of this type of C_6F_5 group not metal bonded can be easily detected by IR spectroscopy.

It is worth noting that in all cases the formation of the $PPh_2C_6F_5$ ligand implies the breaking of M−C bonds. The formation of complexes **3a**−**c** corresponds to a very unusual and rare process, because it requires a reductive coupling between a phosphido ligand and a pentafluorophenyl group to afford a coordinated tertiary phosphane. Although it is well known[15−22] that tertiary phosphane ligands can be transformed thermally to bridging phosphido species through a P−C bond activation and formation of new M−P and M−C bonds, the reverse process is rare. A cluster-mediated conversion of $M-C_6H_5$ into a $P-C_6H_5$ bond, through coupling of a bridging PPh_2 moiety and a phenyl group to give PPh_3, was reported by Braunstein et al.[23] On the other hand, we have reported the elimination process of chloride ligands from $[\{(C_6F_5)_2Pt(\mu\text{-}PPh_2)_2M(\mu\text{-}Cl)\}_2]^{2-}$ (M = Pt, Pd).[4,10] Only for the hetero-tetranuclear derivative is a similar reductive coupling observed, yielding $[Pt_2Pd_2(\mu\text{-}PPh_2)_3(C_6F_5)_3(PPh_2C_6F_5)]$. Considering that the M−C_6F_5 bonds are more stable that the corresponding

(4) Falvello, L. R.; Forniés, J.; Fortuño, C.; Martín, A.; Martínez-Sariñena, A. P. *Organometallics* **1997**, *16*, 5849−5856.
(5) Usón, R.; Forniés, J.; Espinet, P.; Lalinde, E.; Jones, P. G.; Sheldrick, G. M. *J. Chem. Soc., Dalton Trans.* **1982**, 2389−2395.
(6) Ara, I.; Forniés, J.; García, A.; Gómez, J.; Lalinde, E.; Moreno, M. T. *Chem. Eur. J.* **2002**, *8*, 3698−3716.
(7) Usón, R.; Fornies, J.; Espinet, P.; Lalinde, E. *J. Organomet. Chem.* **1983**, *254*, 371−379.
(8) Falvello, L. R.; Forniés, J.; Fortuño, C.; Durán, F.; Martín, A. *Organometallics* **2002**, *21*, 2226−2234.
(9) Alonso, E.; Forniés, J.; Fortuño, C.; Martín, A.; Orpen, A. G. *Organometallics* **2001**, *20*, 850−859.
(10) Alonso, E.; Forniés, J.; Fortuño, C.; Martín, A.; Orpen, A. G. *Organometallics* **2000**, *19*, 2690−2697.
(11) Alonso, E.; Forniés, J.; Fortuño, C.; Martín, A.; Rosair, G. M.; Welch, A. J. *Inorg. Chem.* **1997**, *36*, 4426−4431.
(12) Alonso, E.; Forniés, J.; Fortuño, C.; Tomás, M. *J. Chem. Soc., Dalton Trans.* **1995**, 3777−3784.
(13) Carty, A. J.; MacLaughlin, S. A.; Nucciarone, D. *Phosphorus-31 NMR Spectroscopy in Stereochemical Analysis*; VCH: 1987.
(14) Alonso, E.; Casas, J. M.; Forniés, J.; Fortuño, C.; Martín, A.; Orpen, A. G.; Tsipis, C. A.; Tsipis, A. C. *Organometallics* **2001**, *20*, 5571−5582.
(15) García, G.; García, M. E.; Melón, S.; Riera, V.; Ruiz, M. A.; Villafañe, F. *Organometallics* **1997**, *16*, 624−631.
(16) Shiu, K. B.; Jean, S. W.; Wang, S. L.; Liao, F. L.; Wang, J. C.; Liou, L. S. *Organometallics* **1997**, *16*, 114−119.
(17) Dubois, R. A.; Garrou, P. E. *Organometallics* **1986**, *5*, 460−466.
(18) Bender, R.; Braunstein, P.; Dedieu, A.; Ellis, P. D.; Huggins, B.; Harvey, P. D.; Sappa, E.; Tiripicchio, A. *Inorg. Chem.* **1996**, *35*, 1223−1234.
(19) Mizuta, T.; Onishi, M.; Nakazono, T.; Nakazawa, H.; Miyoshi, K. *Organometallics* **2002**, *21*, 717−726.
(20) Geoffroy, G. L.; Rosenberg, S.; Shulman, P. M.; Whittle, R. R. *J. Am. Chem. Soc.* **1984**, *106*, 1519−1521.
(21) Shulman, P. M.; Burkhardt, E. D.; Lundquist, E.; Pilato, R. S.; Geoffroy, G. L.; Rheingold, A. L. *Organometallics* **1987**, *6*, 101−109.
(22) Zhuravel, M. A.; Moncarz, J. R.; Glueck, D. S.; Lam, K.-C.; Rheingold, A. L. *Organometallics* **2000**, *19*, 3447−3454.
(23) Archambault, C.; Bender, R.; Braunstein, P.; Decian, A.; Fischer, J. *Chem. Commun.* **1996**, 2729−2730.

$M-C_6H_5$ bonds,[24] the reductive coupling should be expected to be a very unusual and unfavorable process.

Surprisingly, treatment of **3a** with $AgClO_4$ in CH_2Cl_2 (molar ratio 1:1) results in the expected precipitation of AgI and the isolation of a yellow solid, which was identified (^{19}F and ^{31}P NMR spectroscopy) as the Pt(III) binuclear derivative **2** (73% yield). Obviously, this very unusual reaction corresponds to a formal intramolecular oxidative addition of $PPh_2C_6F_5$ to a binuclear Pt(II)−Pt(II) moiety resulting in the formation of the binuclear Pt(III)−Pt(III) compound. The reaction is promoted by eliminating the bridging I^- ligand, which induces the $P-C_6F_5$ bond activation and the intermetallic Pt(III)−Pt(III) bond formation. Remarkably, the conversion of $[(C_6F_5)_2Pt(\mu\text{-}PPh_2)_2Pt(C_6F_5)_2]$ to $[(C_6F_5)_2Pt(\mu\text{-}PPh_2)(\mu\text{-}I)Pt(C_6F_5)(PPh_2C_6F_5)]^-$, or vice versa, corresponds to a totally reversible process induced by the presence or absence of I^- anions under very mild conditions.

Surprisingly, although complexes **3b** and **3c** react with $AgClO_4$, they do not render the elusive complexes **2b** and **2c**. The NMR spectra of the reaction products indicated that in both cases a complicated mixture of complexes has been obtained. It is also evident that the $PPh_2C_6F_5$ ligand is still present in the mixture. Attempts to separate and identify all components of the mixtures were unsuccessful.

Despite the well-known activation of the P−C bond in standard phenyl-containing phosphanes by transition metals, the corresponding cleavage of the P−C(fluoroaryl) bond is a very rare event.[25,26] A clean example of a transition metal-mediated $P-Ar_F$ cleavage in a tertiary phosphane has recently been reported.[27] In this case the $P-C_6F_5$ bond cleavage seems to be a consequence of a formal oxidative addition to a Pd(0) intermediate yielding the Pd(II) dimer $[Pd_2(C_6F_5)_2\{\mu\text{-}P(C_6F_5)CH_2CH_2P(C_6F_5)_2\}_2]$. Interestingly, neither the analogous platinum(0) complex nor a platinum(II) derivative appears to undergo this type of P−C bond cleavage even at high temperature.[27] In contrast, the transformation of **3a** to **2** corresponds to an oxidative addition process on Pt(II) metal centers and takes place under very mild conditions. Obviously, the elimination of a four-electron ligand from an anionic binuclear Pt(II) complex affords a coordinatively unsaturated complex in which the oxidative addition of a tertiary phosphane ligand yields a diphenylphosphido bridging ligand with concomitant formation of a $Pt-C_6F_5$ bond.

Considering the outlying processes, it seems sensible to assume that the oxidation of the binuclear $[NBu_4]_2[(C_6F_5)_2M(\mu\text{-}PPh_2)_2M'(C_6F_5)_2]$ complexes with I_2 results in the formation of the binuclear M(III)−M′(III) complexes, which in the presence of I^- decompose very fast for complexes containing Pd, through a reductive coupling of PPh_2 and C_6F_5 and forming $PPh_2C_6F_5$. This process is sufficiently slow at low temperature for the diplatinum complex, thereby allowing its isolation. Of, perhaps, greater interest is the fact that for the diplatinum complex the intramolecular reductive coupling and the reversible oxidative addition processes are induced by the addition to or elimination from the iodide ligand. It is worth noting that Cabeza et al.[28] reported the first demonstration of this type of reversibility in a trinuclear $[Ru_3]^+$ complex. In this case there are P−C(phenyl) bond breaking and bond formation, while in our complex the reversible process implies a P−C(perfluorophenyl) bond.

The spectroscopic data of **3a**, **3b**, and **3c** indicate that all species display similar structures; thereby only the structure of **3b** has been established by an X-ray diffraction study.

2. Crystal Structure of $[(C_6F_5)_2Pd(\mu\text{-}PPh_2)(\mu\text{-}I)Pd(C_6F_5)(PPh_2C_6F_5)]^-$. The structure of complex **3b** together with the atom-labeling scheme is shown in Figure 1, while selected bond distances and angles are listed in Table 1.

The anion of **3b** is a dinuclear complex in which two palladium atoms are linked through an asymmetric bridging system formed by a diphenylphosphido and an iodide ligand. Both palladium atoms lie in conventional square planar environments formed, besides the bridging ligands, by two pentafluorphenyl groups for Pd(1) and one C_6F_5 ligand and the $PPh_2C_6F_5$, a phosphane ligand formed during the reaction process as previously observed.[4] The best least squares planes of the two palladium atoms form an angle of 122.8°.

The intermetallic distance is 3.285(1) Å, which excludes any Pd···Pd interaction. The Pd(1)−P(1)−Pd(2) angle is 90.66(8)°, and the P(1)−Pd−I angles are somewhat narrower (ca. 83°, see Table 1) than expected for an idealized square planar geometry for the coordination environments. Both Pd−I distances have the

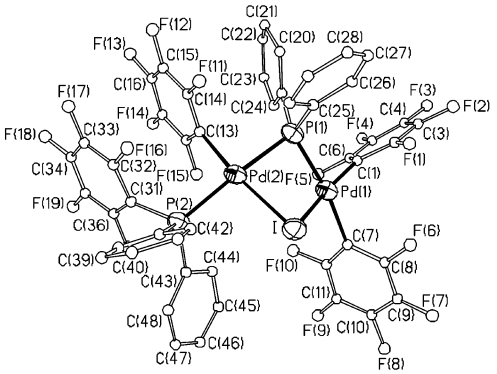

Figure 1. Structure of complex **3b** together with the atom-labeling scheme.

Table 1. Selected Bond Distances [Å] and Angles [deg] and Their Estimated Standard Deviations for 3b

Bond Distances					
Pd(1)−C(1)	2.007(8)	Pd(1)−C(7)	2.099(9)	Pd(1)−P(1)	2.306(2)
Pd(1)−I	2.6899(8)	Pd(2)−C(13)	2.031(8)	Pd(2)−P(1)	2.314(2)
Pd(2)−P(2)	2.377(2)	Pd(2)−I	2.6899(8)		

Bond Angles			
C(1)−Pd(1)−C(7)	89.7(3)	C(1)−Pd(1)−P(1)	95.7(2)
C(7)−Pd(1)−P(1)	170.7(2)	C(1)−Pd(1)−I	167.8(3)
C(7)−Pd(1)−I	92.8(2)	P(1)−Pd(1)−I	83.43(6)
C(13)−Pd(2)−P(1)	89.4(2)	C(13)−Pd(2)−P(2)	93.0(2)
P(1)−Pd(2)−P(2)	175.38(8)	C(13)−Pd(2)−I	171.9(2)
P(1)−Pd(2)−I	83.29(6)	P(2)−Pd(2)−I	94.08(6)
Pd(1)−I−Pd(2)	75.27(2)		

Downloaded by NAT LIB UKRAINE on July 4, 2009
Published on March 18, 2004 on http://pubs.acs.org | doi: 10.1021/om034236y

(24) Usón, R.; Forniés, J.; Tomás, M. *J. Organomet. Chem.* **1988**, *358*, 525−543.
(25) Fahey, D. R.; Mahan, J. E. *J. Am. Chem. Soc.* **1976**, *98*, 4499−4503.
(26) Ang, H. G.; Kwik, W. L.; Leong, W. K.; Johnson, B. F. G.; Lewis, J.; Raithby, P. R. *J. Organomet. Chem.* **1990**, *396*, C43.
(27) Heyn, R. H.; Gorbitz, C. H. *Organometallics* **2002**, *21*, 2781−2784.
(28) Cabeza, J. A.; del Río, I.; Riera, V.; García-Granda, S.; Sanni, B. *Organometallics* **1997**, *16*, 1743−1748.

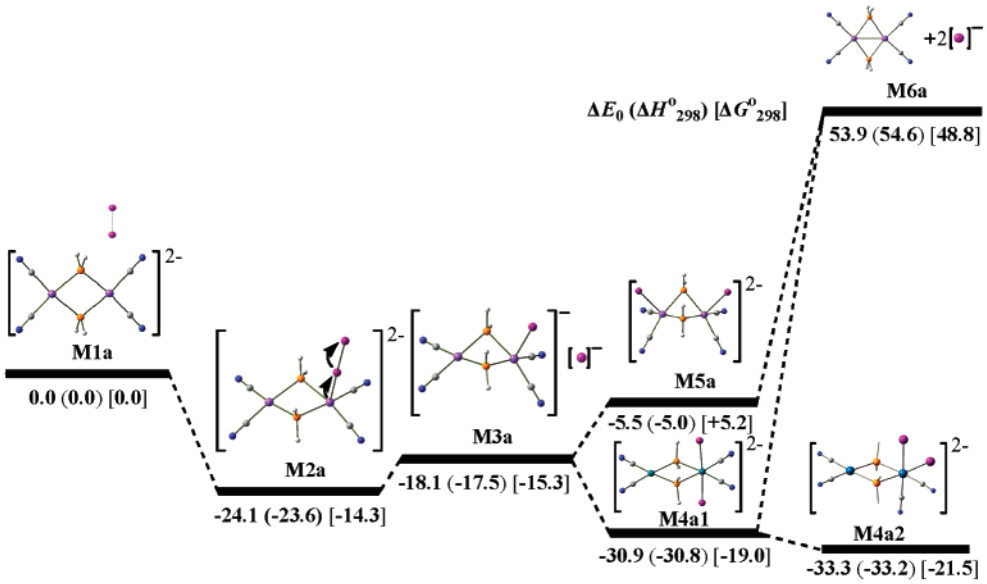

Figure 2. Geometric and energetic profile of the oxidative addition of I_2 to $[(CN)_2Pt(\mu\text{-}PH_2)_2Pt(CN)_2]^{2-}$, **M1a**, yielding the neutral $[(CN)_2Pt(\mu\text{-}PH_2)_2Pt(CN)_2]$ complex, **M6a**. Relative energies (in kcal/mol) at 0 K (ΔE_0). Values in parentheses are reaction enthalpies at 298 K ($\Delta H°_{298}$), and values in square brackets are Gibbs free energies at 298 K ($\Delta G°_{298}$).

Downloaded by NAT LIB UKRAINE on July 4, 2009
Published on March 18, 2004 on http://pubs.acs.org | doi: 10.1021/om034236y

same value, 2.690(1) Å, which is in the range usually found.[5,29−38] On the other hand, the Pd(1)−I−Pd(2) angle is only 75.7(2)°, which is one of the smallest values for these kinds of bridging systems. Finally, to the best of our knowledge, this is the first complex characterized by X-ray diffraction in which there is only one iodide bridging ligand, the common trend being the existence of a symmetric double iodide bridging system.

In an attempt to learn more about these peculiar intramolecular reversible processes we searched thoroughly the potential energy surfaces of the respective reactions through electronic structure calculations based on density functional theory (DFT) methods, and the geometric and energetic profile of the reactions in a vacuum will be discussed herein.

3. Modeling the Intramolecular Reductive Coupling in the $[(CN)_2M(\mu\text{-}PH_2)_2M'(CN)_2]$ (M = M′ = Pt or Pd, M = Pt, M′ = Pd) Complexes Promoted by I^- Anions in a Vacuum. The primary scope of this part is to furnish details on the mechanism of the intramolecular reductive coupling of a μ-PPh_2 bridging ligand and a coordinated C_6F_5 group as well as the reversible intramolecular oxidative addition of a coordinated $PPh_2C_6F_5$ ligand in the $[(CN)_2M(\mu\text{-}PH_2)_2M'(CN)_2]/[(CN)_2M(\mu\text{-}PH_2)(\mu\text{-}I)M'(CN)(PH_2CN)]^-$ (M = M′ = Pt or Pd, M = Pt, M′ = Pd) redox couples. To accomplish this, the potential energy surfaces (PES) of the respective reactions of appropriately selected model compounds with computationally convenient size were computed by DFT methods (see Computational Methods), as these methods have extensively been applied to inorganic problems, and the accuracy of the calculated structural and energetic parameters has been demonstrated for a variety of systems, including organometallic compounds.[39,40] To denote the model compounds we will use labels such as **M1a**, **M1b**, etc.

3.1. Oxidation of the $[(CN)_2M(\mu\text{-}PH_2)_2M'(CN)_2]^{2-}$ (M = M′ = Pt or Pd, M = Pt, M′ = Pd) Complexes by I_2 in a Vacuum. The energetic and geometric profiles of the oxidative addition of I_2 to one of the metal centers in the $[(CN)_2M(\mu\text{-}PH_2)_2M'(CN)_2]^{2-}$ (M = M′ = Pt, **M1a**; M = Pt, M′ = Pd, **M1b**; and M = M′ = Pt, **M1c**) complexes are presented in Figures 2, 3, and 4.

In general terms, the oxidation processes of the Pt_2 (**M1a**), PtPd (**M1b**), and Pd_2 (**M1c**) species follow analogous reaction pathways, but with a noticeable difference concerning the final product formed in the case of the Pd_2 species. Thus, in the first step of the oxidative addition reaction the I_2 molecule interacts with one of the four-coordinate metal centers of **M1a** (Figure 2), **M1b** (Figure 3), and **M1c** (Figure 4) aligned perpendicularly to the coordination plane, yielding the five-coordinate intermediates, **M2a**, **M2b1** or **M2b2**, and **M2c**, respectively, with square pyramidal stereochemistry. The intermediates **M2a**, **M2b1**, **M2b2**, and **M2c** are stabilized with respect to the reactants by 24.1, 24.9, 21.5, and 22.4 kcal/mol, respectively. It is worth noting that the coordination of the iodine ligand to Pt(II) in **M1b** (Figure 3a) is slightly favored with respect to its coordination to the Pd(II) metal center (Figure 3b). This could easily be explained in terms of the orbital interac-

(29) Donde, Y.; Overman, L. E. *J. Am. Chem. Soc.* **1999**, *121*, 2933−2934.
(30) Rheingold, A. L.; Fultz, W. C. *Organometallics* **1984**, *3*, 1414−1417.
(31) Maassarani, F.; Pfeffer, M.; Le Borgne, G. *Organometallics* **1987**, *6*, 2043−2053.
(32) Smith, D. C.; Lake, C. H.; Gray, G. M. *Chem. Commun.* **1998**, 2771−2772.
(33) Brunet, L.; Mercier, F.; Ricard, L.; Mathey, F. *Angew. Chem., Int. Ed. Engl.* **1994**, *33*, 742−745.
(34) Grushin, V. V.; Alper, H. *Organometallics* **1993**, *12*, 1890−1901.
(35) Crispini, A.; Ghedini, M.; Neve, F. *J. Organomet. Chem.* **1993**, *448*, 241−245.
(36) Marshall, W. J.; Young, R. J.; Grushin, V. V. *Organometallics* **2001**, *20*, 523−533.
(37) Neve, F.; Crispini, A.; Francescangeli, O. *Inorg. Chem.* **2000**, *39*, 1187−1194.
(38) Ryabov, A. D.; Kuzmina, L. G.; Polyakov, V. A.; Kazankov, G. M.; Ryabova, E. S.; Pfeffer, M.; Vaneldik, R. *J. Chem. Soc., Dalton Trans.* **1995**, 999−1006.
(39) Ziegler, T. *Chem. Rev.* **1991**, *91*, 651−667.
(40) Mire, L. W.; Wheeler, S. D.; Wagenseller, E.; Marynick, D. S. *Inorg. Chem.* **1998**, *37*, 3099−3106.

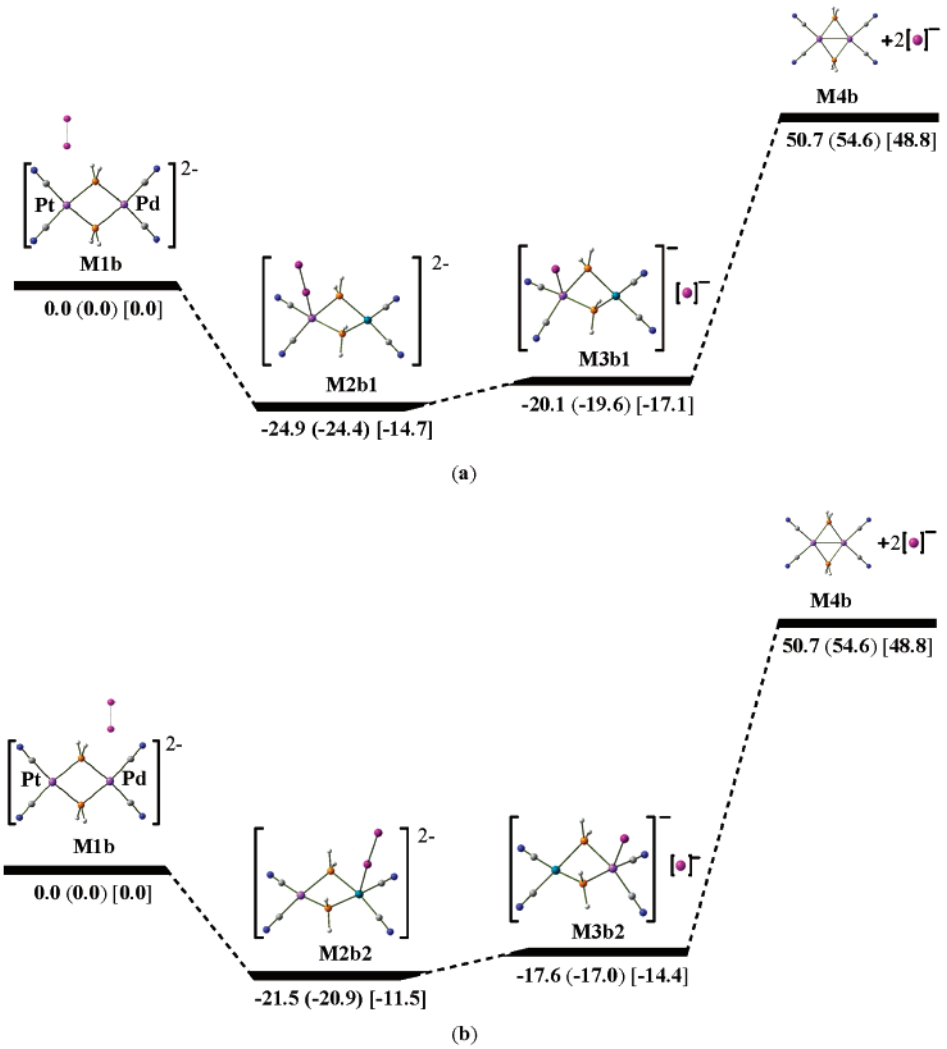

Figure 3. Geometric and energetic profile of the oxidative addition of I_2 to $[(CN)_2Pt(\mu\text{-}PH_2)_2Pd(CN)_2]^{2-}$, **M1b**, either to Pt (a) or Pd (b) central atoms, yielding the neutral $[(CN)_2Pt(\mu\text{-}PH_2)_2Pd(CN)_2]$ complex, **M4b**. Relative energies (in kcal/mol) at 0 K (ΔE_0). Values in parentheses are reaction enthalpies at 298 K ($\Delta H°_{298}$), and values in square brackets are Gibbs free energies at 298 K ($\Delta G°_{298}$).

Downloaded by NAT LIB UKRAINE on July 4, 2009
Published on March 18, 2004 on http://pubs.acs.org | doi: 10.1021/om034236y

tions responsible for the association of the iodine molecule to the metal center.

In all binuclear complexes there are favorable orbital interaction between their HOMO or HOMO-1, which correspond to nonbonding molecular orbitals (MOs) localized mainly on one of the metal centers (essentially d_{z^2} orbitals), and the LUMO of I_2, which corresponds to an antibonding σ^*_{I-I} MO. In the **M2b1** intermediate the σ^* LUMO of the iodine ligand interacts with the HOMO-1 of **M1b**, which is an almost pure d_{z^2} orbital localized on the Pt(II) metal center, whereas in **M2b2** the σ^* LUMO of the iodine ligand interacts with the HOMO-2 of **M1b**, which corresponds to an antibonding combination of two d_{z^2} orbitals localized on both the Pd(II) and Pt(II) metal centers with nearly the same contribution.

The n(Pt) → σ^*_{I-I} MO or n(Pd) → σ^*_{I-I} MO orbital interactions favor the transfer of the nonbonding electron pair belonging to the Pt(II) or Pd(II) metal centers to the antibonding σ^*_{I-I} MO, leading to a two-electron (2e) oxidation of the metal center and the concomitant rupture of the I−I bond, because of accumulation of the transferred electron density on the antibonding σ^*_{I-I} MO. The electron transfer proceeds uphill on the potential energy surface, without an intervening transition state demanding about 6.0, 4.8, 3.9, and 2.7 kcal/mol in terms of ΔE_0 for **M2a**, **M2b1**, **M2b2**, and **M2c**, respectively. Notice that the coordinated iodine donor atom remains coordinated to the metal center of **M2a**, **M2b1**, **M2b2**, and **M2c** as an iodide ligand during the course of the electron transfer process, yielding the binuclear complexes **M3a**, **M3b1**, **M3b2**, and **M3c**, respectively, with the oxidized metal center being five-coordinate.

The equilibrium geometries of all stationary points involved in the oxidative addition of I_2 to **M1a**, **M1b**, and **M1c**, computed at the B3LYP/LANL2DZ level of theory, are shown in the Supporting Information (Figures S1, S2, and S3, respectively). In general terms, the substitution of one of the two Pt metal centers in **M1a** with Pd to afford **M1b** does not alter significantly the equilibrium geometries of the species involved in the oxidation process; therefore only the salient features of their geometries will be discussed herein.

There are no metal−metal interactions in **M1a**, **M1b** (Pt···Pt and Pt···Pd distances of 3.863 and 3.864 Å, respectively), and **M1c** (Pd···Pd distance of 3.850 Å); thereby a 16 valence electron count is obtained for each

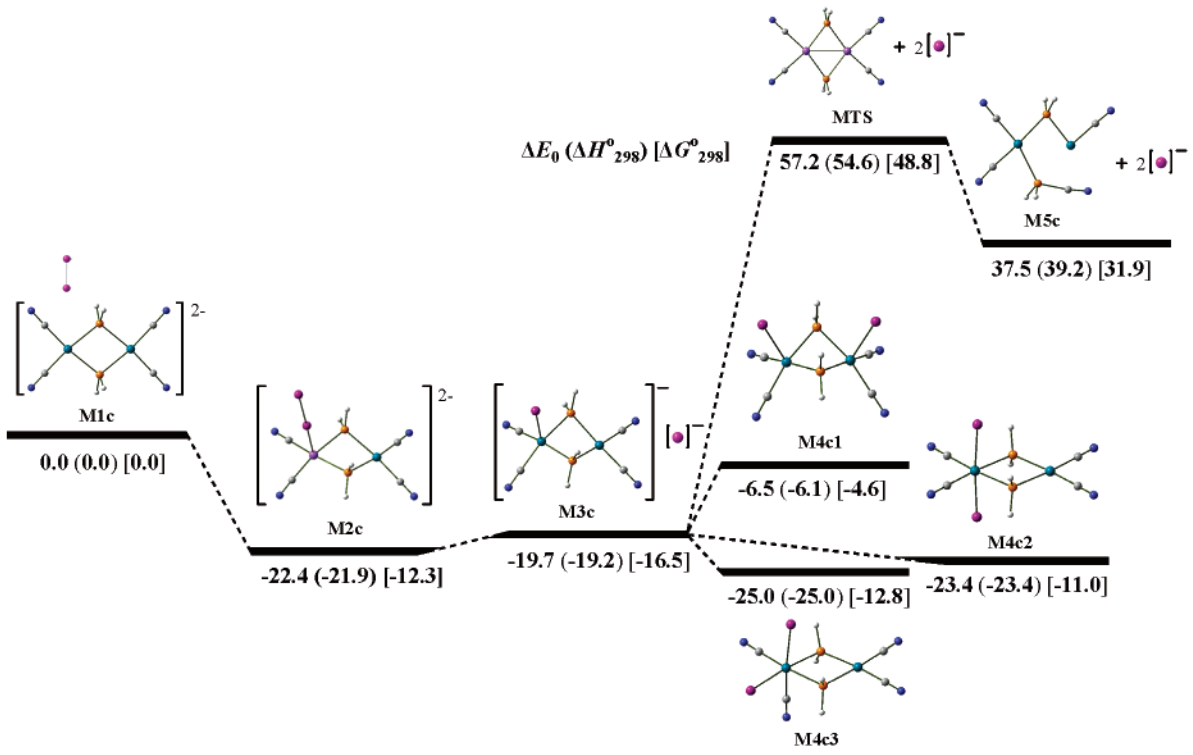

Figure 4. Geometric and energetic profile of the oxidative addition of I_2 to $[(CN)_2Pd(\mu\text{-}PH_2)_2Pd(CN)_2]^{2-}$. Relative energies (in kcal/mol) at 0 K (ΔE_0). Values in parentheses are reaction enthalpies at 298 K ($\Delta H°_{298}$), and values in square brackets are Gibbs free energies at 298 K ($\Delta G°_{298}$).

metal center which adopts a distorted square planar coordination environment with small P−Pt−P and P−Pd−P bond angles of about 77°. The calculated structural parameters of **M1a** compare favorably to the experimental and theoretical data of **1a** reported previously.[3]

Intermediates **M2a**, **M2b1**, **M2b2**, and **M2c** exhibit analogous geometries corresponding to a loose end-on association of the I_2 molecule with one of the metal centers of **M1a**, **M1b**, and **M1c** in a perpendicular way, thus forcing the metal center to adopt a square pyramidal stereochemistry with the I_2 ligand in the apical position. The calculated Pt−I and Pd−I bond lengths of about 2.91 Å are indicative of the weak interaction, which is also reflected in the computed interaction energies of 21−25 kcal/mol in terms of ΔE_0. Notice that the Pt···I and Pd···I bond distances are much smaller than the sum of the van der Waals radii of both atoms, 3.9 Å.[41]

Generally, the association of the I_2 molecule to the metal center does not introduce significant structural changes except for the characteristic folding of the $M(\mu\text{-}PH_2)_2M'$ (M = M′ = Pt or Pd; M = Pt, M′ = Pd) cores with flap angles in the range 146−155°. The folding along the P···P axis imposes a narrowing of the M−P−M′ bond angles and a shortening of the M···M′ separation distances. Interestingly there is a significant elongation of the I−I bond amounting to about 0.25−0.26 Å for all species (the computed I−I bond length of the free I_2 ligand is 2.863 Å at the same level of theory). This is expected in terms of the favorable $n(Pt) \rightarrow \sigma^*_{I-I}$ and $n(Pd) \rightarrow \sigma^*_{I-I}$ MO orbital interactions associated with a charge transfer (CT) from the metal center to the coordinated I_2 molecule. The stabilization energy $\Delta E_{(2)}$ associated with the charge transfer interactions between the relevant donor−acceptor orbitals computed from the second-order perturbative estimates of the Fock matrix in the natural bond orbital (NBO) analysis[42] allows these specific interactions to be pinpointed. The stabilization energy of 28.4, 28.1, 18.1, and 17.2 kcal/mol introduced by the favorable $n(Pt) \rightarrow \sigma^*_{I-I}$ MO or $n(Pd) \rightarrow \sigma^*_{I-I}$ MO orbital interactions in **M2a**, **M2b1**, **M2b2**, and **M2c**, respectively, accounts well for the elongation of the σ I−I bond. Noteworthy is the remarkable lowering of the occupancy of one of the 5d or 4d lone pairs of the oxidized platinum or palladium centers; the computed occupancies were 1.710, 1.712, 1.771, and 1.781 for **M2a**, **M2b1**, **M2b2**, and **M2c** intermediates, respectively. Moreover, the natural charges on the metal centers were found in the range of 0.27−0.44 charge units, while the coordinated and terminal iodine atoms acquire negative natural charges of −0.01 to −0.06 and −0.40 charge units, respectively.

The computed Pt−I or Pd−I bond dissociation energies (BDE) of 72.0, 70.8, 68.3, and 76.9 kcal/mol indicate strong interactions of the apical iodide ligand with the Pt or Pd centers of **M3a**, **M3b1**, **M3b2**, and **M3c** intermediates, respectively. The natural charges on the metal centers of **M3a**, **M3b1**, **M3b2**, and **M3c** intermediates were found in the range 0.30−0.48 charge units, while the iodide ligand acquires a negative natural charge of −0.11 to −0.22 charge units. The charge density distribution on the metal centers illustrates their different oxidation states, with the five-coordinated one exhibiting the higher oxidation state.

(41) Huheey, J. E.; Keiter, E. A.; Keiter, R. L. *Inorganic Chemistry*, 4th ed.; Harper: New York, 1993.

(42) Weinhold, F. In *The Encyclopedia of Computational Chemistry*; Schleyer, P. v. R., Ed.; John Wiley & Sons: Chichester, 1998; pp 1792−1811.

Downloaded by NAT LIB UKRAINE on July 4, 2009
Published on March 18, 2004 on http://pubs.acs.org | doi: 10.1021/om034236y

Downloaded by NAT LIB UKRAINE on July 4, 2009
Published on March 18, 2004 on http://pubs.acs.org | doi: 10.1021/om034236y

Scheme 3

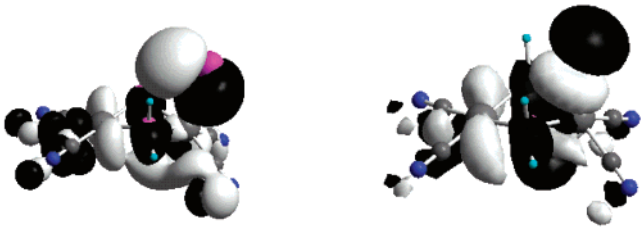

In the oxidized complexes **M3a** and **M3c** we further examined the possibility for the iodide anion resulting from the rupture of the I−I bond to be coordinated to either Pt(IV) or Pt(II) and Pd(IV) or Pd(II) metal centers, thus affording the isomeric species **M4a1, M4a2** or **M5a**, and **M4c1**, **M4c2**, or **M4c3**, respectively. The coordination of the second iodide ligand to the Pt(IV) metal center of **M3a** or to the Pd(IV) metal center of **M3c** either in axial or equatorial coordination sites corresponds to an exothermic process, with a computed reaction enthalpy of −13.3, −15.7, −4.2, and −5.8 kcal/mol, respectively. In contrast, the coordination to Pt(II) or Pd(II) metal centers corresponds to an endothermic process, with a reaction enthalpy of 12.5 and 13.1 kcal/mol. Looking at the frontier molecular orbitals of **M3a** (Scheme 3) it can be seen that the LUMO, which is the acceptor orbital to accommodate the lone pair of electrons of the incoming iodide ligand, is a σ^*_{Pt-I} MO corresponding to the out-of-phase combination of the d_{z^2} AO of Pt(IV) and the p AO of the iodide ligand. It is obvious then why the formation of **M4a1** or **M4a2** is favored with respect to the formation of **M5a**.

The salient feature of the optimized structures **M4a1** and **M4c2** is the planarity of the cyclic Pt(II)(μ-PH_2)$_2$-Pt(IV) and Pd(II)(μ-PH_2)$_2$Pd(IV) frameworks, respectively. The M(II)···M(IV) distances of 3.850 and 3.817 Å in **M4a1** and **M4c2**, respectively, do not support intermetallic interactions. The M(II) center is four-coordinated with a square planar stereochemistry, while the M(IV) one is six-coordinated with a distorted octahedral stereochemistry.

Although the coordination of the iodide ligands to Pt(II) and Pt(IV) or Pd(II) and Pd(IV) centers is responsible for the equalization of the oxidation states of the two platinum or palladium centers to an intermediate oxidation state, their removal is a prerequisite to obtain the final oxidized products **M6a** and **M5c**, respectively. Noteworthy is the different behavior of the dipalladium complex in this stage of the reaction pathway, as compared to the Pt_2 and PdPt analogues. Despite the weakening of the Pt−I bonds in **M5a**, their dissociation is still an energy-consuming process with a reaction enthalpy of 59.6 kcal/mol. Complex **M6a** is a planar dinuclear Pt(III) complex involving strong intermetallic Pt···Pt interactions with a Pt···Pt separation distance of 2.844 Å. Surprisingly, on the other hand, the final iodide-free dinuclear Pd(III)−Pd(III) complex corresponds to a saddle point (transition state, **MTS**), which readily converts to a more stable Pd(II)−Pd(II) complex **M5c** through a reductive coupling of one of the CN ligands with one of the bridged phosphido ligands. Complex **M5c** is stabilized with respect to **MTS** by 19.7 kcal/mol, while on the whole the Pd−I bond dissociation and the concomitant reductive coupling are energy-consuming processes, the reaction enthalpy being equal to 57.2 kcal/mol. Finally, in the planar dinuclear Pt(III)−Pd(III) complex **M4b** the Pt···Pd separation distance of 2.821 Å is indicative of strong intermetallic Pt···Pd interactions. These interactions are clearly shown in the respective MOs given in Scheme 4.

Scheme 4

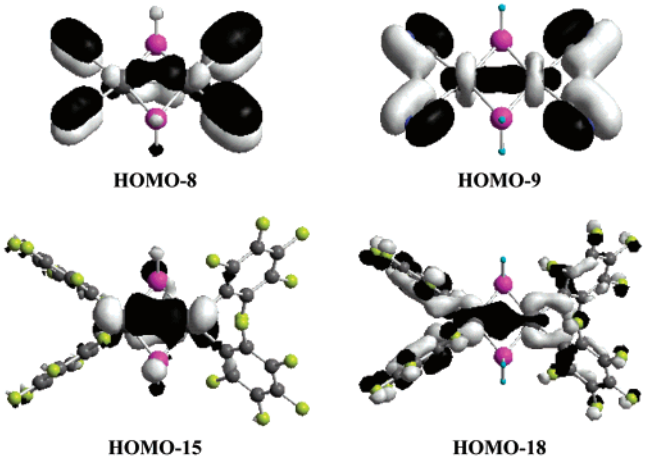

It is worth noting that the CN ligands coordinated to the Pd central atom in **M4b** are closer to the P donor atom of the bridged phosphido ligand (P···C separation distance of 2.84 Å) than the CN ligands coordinated to Pt central atom (P···C separation distance of 2.96 Å). This configuration seems to favor the reductive coupling between the two ligands to form the new PH_2(CN) ligand coordinated to the Pd metal center. The same holds true for complex **M7** representing the real-life complex (Figure S2).

Finally, it should be noted that the predicted thermodynamic stability of the oxidized products **M6a**, **M4b**, and **M5c** (by about 50 kcal/mol) is not consistent with the experimental observation that the 2*e* oxidation process takes place at very low temperature (−70 °C). Control calculations using a larger basis set, e.g., LANL2DZ for the metal and iodine atoms and 6-31G(d,p) for the rest of the non-metal atoms, hoping to obtain more reliable energies did not improved the results obtained at the B3LYP/LANL2DZ level. Thus, for example the predicted thermodynamic stability of complex **M6a** is about 46 kcal/mol using the larger basis set. The phenomenal inconsistency between theory and experiment is not surprising considering the poor modeling of the experimental redox behavior in the gas phase. Actually, this is the case for analogous multielectron redox reactions accompanied by a reversible structural change, where it was found that the inclusion of solvation was necessary to correctly predict the energetic reaction profile.[43] Unfortunately, due to our present computational resources and the extremely high CPU demands, the investigation of the macroscopic influence of the solvent on the energetics of the redox reactions was not possible to perform. The electrostatic effects of the bulk environment are expected to play an important role in stabilizing the various charged species along the reaction pathway.

3.2. Intramolecular Reductive Coupling in the [(CN)$_2$M(μ-PH$_2$)$_2$M′(CN)$_2$] (M = M′ = Pt or Pd, M =

(43) Baik, M.-H.; Ziegler, T.; Schauer, C. K. *J. Am. Chem. Soc.* **2000**, *125*, 9143−9154, and references therein.

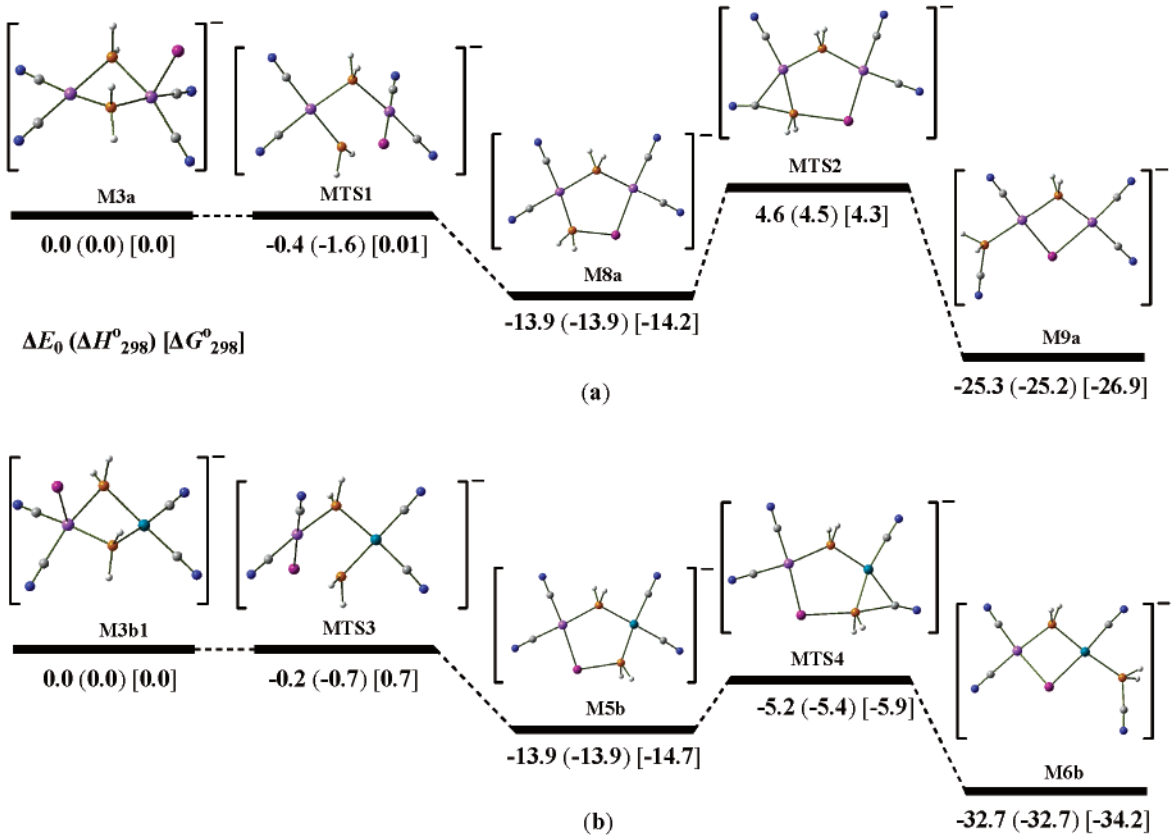

Figure 5. Geometric and energetic profiles of the intramolecular reductive coupling in $[(CN)_2Pt(\mu\text{-}PH_2)_2Pt(CN)_2]$ (a) and $[(CN)_2Pt(\mu\text{-}PH_2)_2Pd(CN)_2]$ (b) promoted by I^- anions. Relative energies (in kcal/mol) at 0 K (ΔE_0). Values in parentheses are reaction enthalpies at 298 K ($\Delta H°_{298}$), and values in square brackets are Gibbs free energies at 298 K ($\Delta G°_{298}$).

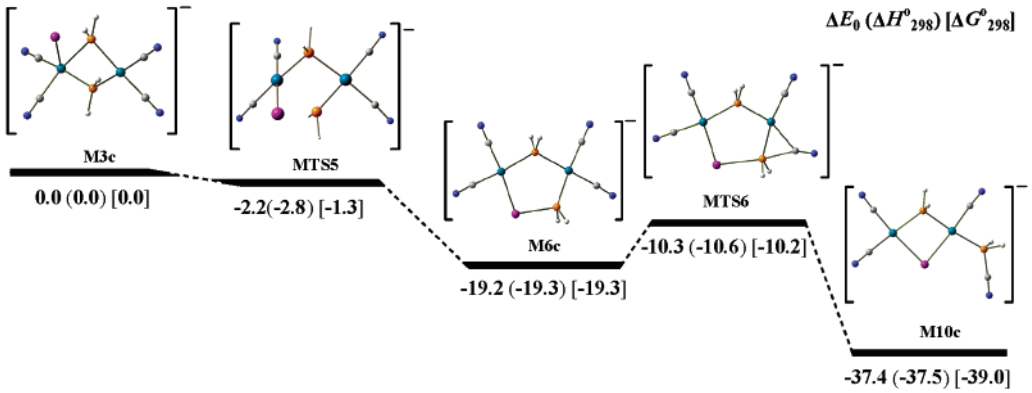

Figure 6. Geometric and energetic profile of the intramolecular reductive coupling in the course of the oxidation of $[(CN)_2Pd(\mu\text{-}PH_2)_2Pd(CN)_2]^{2-}$ with iodine. Relative energies (in kcal/mol) at 0 K (ΔE_0). Values in parentheses are reaction enthalpies at 298 K ($\Delta H°_{298}$), and values in square brackets are Gibbs free energies at 298 K ($\Delta G°_{298}$).

Pt, M′ = Pd) Complexes Promoted by I^- Anions in a Vacuum. The energetic and geometric profiles of the intramolecular reductive coupling in the $[(CN)_2Pt(\mu\text{-}PH_2)_2Pt(CN)_2]$ (**M6a**) and $[(CN)_2Pt(\mu\text{-}PH_2)_2Pd(CN)_2]$ (**M4b**) complexes promoted by I^- anions are depicted schematically in Figure 5, while those of the intramolecular reductive coupling taking place in the course of the oxidative addition of I_2 to the $[(CN)_2Pd(\mu\text{-}PH_2)_2Pd(CN)_2]^{2-}$ (**M1c**) complex are shown in Figure 6. The equilibrium geometries of the species involved in the intramolecular reductive coupling in **M6a** and **M4b** promoted by I^- anions and in the course of the oxidative addition of I_2 to **M1c** are shown in the Supporting Information (Figures S4, S5, and S6, respectively).

The initiator of the reductive coupling process for **M6a** is complex **M3a**, formed either by the oxidation of **M1a** with I_2 or via the coordination of the iodide ligand to one of the platinum centers of the oxidized complex **M6a** of the **M1a/M6a** redox couple (Figure 2); the latter is a strongly exothermic process with an exothermicity amounting to −72.0 kcal/mol. On the other hand, the initiator of the reductive coupling process for **M4b** could be either complex **M3b1** or **M3b2**, formed either by the oxidation of **M1b** with I_2 or via the coordination of the iodide ligand to Pt or Pd atoms of the oxidized complex **M4b** (Figure 3); the latter is also a strongly exothermic process with exothermicity of −70.8 and −68.3 kcal/mol, respectively. Since the energetically more favorable

Downloaded by NAT LIB UKRAINE on July 4, 2009
Published on March 18, 2004 on http://pubs.acs.org | doi: 10.1021/om034236y

pathway is that involving the **M3b1** intermediate, we will discuss only the mechanism of the intramolecular reductive coupling process following this pathway. The alternative pathway of the reductive coupling through intermediate **M3b2** is expected to follow the same mechanism without significant changes in both the geometric and energetic profile of the reaction.

Complexes **M3a, M3b1**, and **M3c** readily convert to the more stable intermediates **M8a**, **M5b**, and **M6c** through the transition states **MTS1**, **MTS3**, and **MTS5**, respectively. Noteworthy are the small negative values of the activation barriers, which become even more negative (−3.9, −2.6, and −2.9 kcal/mol for the formation of **M8a**, **M5b**, and **M6c**, respectively) upon enlargement of the basis set (LANL2DZ for the metal and iodine atoms and 6-31G(d,p) for the rest of the nonmetal atoms). It should be noted that the structural parameters of the transition states are only marginally affected upon enlargement of the basis set. It is evident then that a more correlated computational technique could give more realistic activation barriers for the respective processes.

In the following stage a reductive coupling of a bridging μ-PH_2 ligand and a CN^- group takes place, yielding the final products **M9a**, **M6b**, and **M10c** through the transition states **MTS2**, **MTS4**, and **MTS6** with a relatively low activation barrier of 18.5 (14.4), 8.7 (5.6), and 8.9 (6.1) kcal/mol, respectively. The figures in parentheses are the computed activation barriers using the larger basis set. The unexpected intramolecular reductive coupling in **M8a**, **M5b**, and **M6c** corresponds to an exoergic process by 11.4 (13.0), 18.8 (21.8), and 18.2 (21.0) kcal/mol, respectively.

Following the reverse reaction pathway complexes **M9a**, **M6b**, and **M10c** could be converted to intermediates **M8a**, **M5b**, and **M6c** through the transition states **MTS2**, **MTS4**, and **MTS6** with a much higher activation barrier of about 29.9 (27.4), 27.5 (27.4), and 27.1 (27.1) kcal/mol, respectively. Removal of the bridged iodide ligand upon reaction of the final products **M9a** and **M6b** with Ag^+ ions yields the iodide-free complexes **M11** and **M12** (Scheme 5), which are 4.4 and 26.8 kcal/mol more stable than the oxidized products **M6a** and **M4b**, respectively. The higher stability of **M12** with respect to **M4b** strongly suggests that this species should be the final product of the oxidation process, in full agreement with experiment.

The equilibrium geometries of **MTS1**, **MTS3**, and **MTS5** are similar, resulting from the structure of the initiators **M3a, M3b1**, and **M3c**, respectively, upon rupture of one of the Pt−P or Pd−I bonds of the bridged phosphido ligands of the five-coordinated metal center. The Pt−I bond in **MTS1** and **MTS3** is elongated with respect to initiators **M3a** and **M3b1** by 0.087 and 0.081 Å, respectively, while the Pd−I bond in **MTS5** is shortened with respect to **M3c** by 0.045 Å.

The intermediates **M8a, M5b**, and **M6c** adopt similar geometries involving a perfect planar five-membered dimetallacycle ring consisting of the two metal centers, two P atoms, and the iodine heteroatoms. Both metal centers are four-coordinated with square planar coordination environment, which is coplanar with the five-membered ring. The Pt−I bond length in **M8a** does not change significantly, while the Pt−P bond of the iodophosphane ligand is further shortened by about 0.030 Å. This iodophosphane ligand continues to move toward the coordinated CN ligand with the P−Pt−C bond angle being narrowed by about 7°. The most noticeable difference in the structure of **M5b** with respect to that of **M8a** concerns the nonbridged phosphido ligand, which is closer to the coordinated CN ligand than to the Pd(II) center, since both the Pd−P bond and the P−Pd−C bond angles are smaller than the corresponding structural parameters of **M8a**. The transition states **MTS2**, **MTS4**, and **MTS6** exhibit a reactant-like structure involving the planar five-membered ring, while concomitantly the P−CN bond is being formed, yielding a three-membered PtPC or PdPC ring, respectively. The respective Pt−CN and Pd−CN bonds participating in the formation of the three-membered rings have been dramatically elongated by 0.419, 0.311, and 0.316 Å, respectively.

Scheme 5

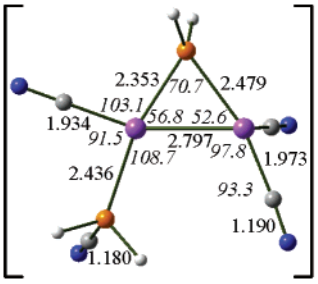

M11

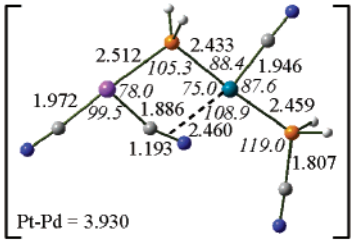

M12

The equilibrium structure of **M11** (Scheme 5) corresponds to a diplatinum complex involving strong Pt···Pt interactions (Pt···Pt separation distance of 2.797 Å). In **M11** both platinum atoms are four-coordinated. However, the platinum atom bearing the PH_2(CN) ligand exhibits a square planar stereochemistry, while the other platinum atom adopts a butterfly configuration. It can be seen that the orientation of the ligands around the two Pt(II) centers in **M11** could support favorable interactions for the intramolecular oxidative addition of the PH_2(CN) moiety to occur, yielding the oxidized product **M6a**. On the other hand, the equilibrium structure of the iodide-free complex **M12** corresponds to a heterodinuclear complex with the Pt(II) and Pd(II) metal centers three-coordinated in a T-shaped configuration. The Pt(II)···Pd(II) distance of 3.930 Å does not indicate metal−metal bonding in **M12**. Moreover, the Pt(II) and Pd(II) metal centers in **M12** acquire a positive natural charge of 0.52 and 0.41 charge units, respectively, indicating that both metal centers exhibit the same oxidation state. Obviously complex **M12** could consist of an alternative intermediate in the reductive

Downloaded by NAT LIB UKRAINE on July 4, 2009
Published on March 18, 2004 on http://pubs.acs.org | doi: 10.1021/om034236y

Downloaded by NAT LIB UKRAINE on July 4, 2009
Published on March 18, 2004 on http://pubs.acs.org | doi: 10.1021/om034236y

Scheme 6

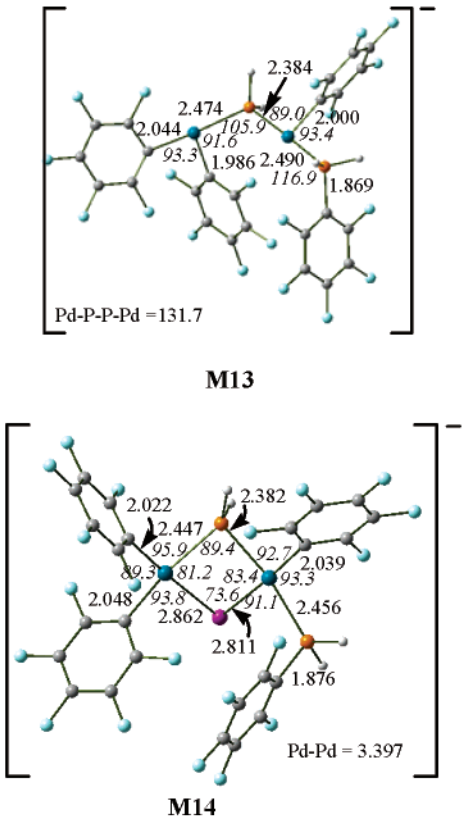

coupling process, since it can easily react with iodide ligands to afford the final product **M6b**.

Considering that both the reductive coupling and the oxidative addition reactions involve the breaking of a Pt−CN bond and the formation of a P−CN bond, we calculated the energies of the respective bonds for the model $[Pt(CN)_2(PH_2)I]^-$ complex and the $PH_2(CN)$ ligand. The Pt−CN and P−CN bond dissociation energies are predicted to be 71.9 and 91.6 kcal/mol, respectively. Obviously, there is an energy gain in the reductive coupling process involving the breaking of the Pt−CN and the formation of the P−CN bond.

Searching the PES of the Pd_2 complex starting with the geometry of a real-life complex $[(C_6F_5)_2Pd(III)(\mu\text{-}PH_2)_2Pd(III)(C_6F_5)_2]$, we found a local minimum corresponding to complex $\{(C_6F_5)_2Pd(II)(\mu\text{-}PH_2)Pd(II)(C_6F_5)\text{-}[PH_2(C_6F_5)]\}$, **M13** (Scheme 6). In effect, the formation of complex **M13** could be the result of the intramolecular reductive coupling of one C_6F_5 ligand with a bridging phosphido ligand, taking place in a "transient", highly unstable, and therefore not isolable dinuclear Pd(III)−Pd(III) complex.

In complex **M13** both Pd(II) centers are three-coordinated with a T-shaped geometry (the P−Pd−P bond angles are about 174°). The Pd(II)···Pd(II) distance of 3.878 Å does not indicate intermetallic interactions. It is clear that complex **M13** could be considered as an alternative intermediate in the reductive coupling process, since it can easily react with iodide ligands to afford the final product **M14** (Scheme 6). Both three-coordinated Pd(II) atoms acquiring a positive natural charge of 0.42 and 0.54 charge units are electrophilic centers; thereby the iodide anions have nearly equal possibility to be coordinated to each one, and under a

Scheme 7

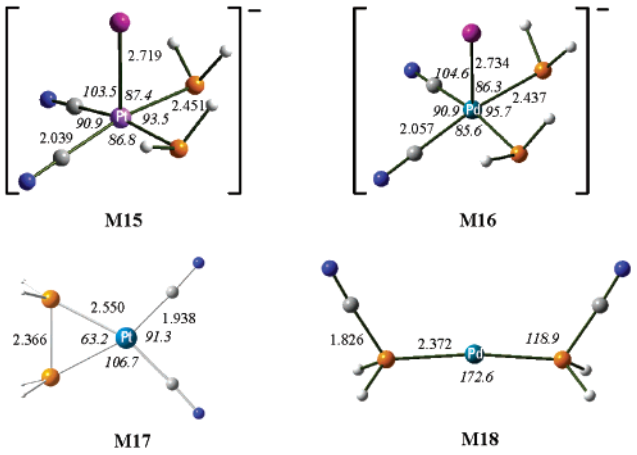

free rotation around the respective Pd−P bond the final product is formed. Irrespective of which of the two Pd(II) centers the iodide ligand would be coordinated to, the formation of the final product corresponds to a strongly exothermic process, with an exothermicity equal to 79.7 kcal/mol.

Noteworthy is the excellent agreement of the computed structure of the final product **M14** with the experimentally determined one by X-ray crystallography. Certainly, one would expect small deviations of some of the computed geometrical parameters with respect to the experimental ones considering that in **M14** the terminal $PPh_2(C_6F_5)$ ligand was replaced by the simpler $PH_2(C_6F_5)$ one.

Finally, to get a deeper insight of the role of the iodide anions in promoting the intramolecular reductive process in the homo- and hetero-dinuclear platinum and palladium complexes we searched the PES of the mononuclear $[M(PH_2)_2(CN)_2]$ and $[M(PH_2)_2(CN)_2(I)]$ (M = Pt, Pd) complexes. For both five-coordinate Pt(IV) and Pd(IV) complexes we located on the PES local minima corresponding to the square pyramidal structures **M15** and **M16** (Scheme 7).

The salient differences of the structures of **M15** and **M16** refer to the M−I and M−P bond lengths. Thus, the Pd−I bond is longer than the Pt−I bond by 0.015 Å, while the Pd−P bond is shorter than the Pt−P bond by 0.014 Å. Upon removing the iodide ligand from **M15** and **M16**, the two complexes responded in a different way. Complex **M15** was transformed to the stable four-coordinate Pt(II) complex **M17** (Scheme 7) with the metal center in a square planar environment involving a diphosphane ligand resulting from the reductive coupling of the two terminal phosphido ligands. On the other hand, complex **M16** was spontaneously transformed to the stable two-coordinate Pd(0) complex **M18** (Scheme 7) exhibiting a slightly bending configuration (P−Pd−P bond angle of 172.6°). Complex **M18** involves two phosphane ligands resulting from the double intramolecular reductive coupling of the CN with the PH_2 ligands. The salient feature of structure **M18** is the shortening of the Pd−P bond by 0.119 Å with respect to the corresponding bond of the dinuclear complex **M10c**. It should be noted that two-coordinate Pd(0) complexes with phosphane ligands are well-known species extensively reported in the literature. In summary theory provides guides for further experimental

Downloaded by NAT LIB UKRAINE on July 4, 2009
Published on March 18, 2004 on http://pubs.acs.org | doi: 10.1021/om034236y

work on these very interesting reductive coupling processes predicted to occur even in mononuclear palladium complexes. Some experimental examples of this process have recently been reported.[44,45]

Conclusions

In this work we have reported a comprehensive study of the two-electron (2*e*) oxidation reactions of the $[NBu_4]_2[(L)_2M(\mu\text{-}PPh_2)_2M'(L)_2]$ (M = M′ = Pt or Pd; M = Pt, M′ = Pd; L = C_6F_5) complexes using I_2 as an oxidant by means of both experimental and electronic structure calculation methods. The electronic structure calculations based on the gradient-corrected (B3LYP) density functional theory were performed on appropriately selected model compounds with computationally convenient size. The results can be summarized as follows.

(i) The oxidation reactions were found to be complex processes involving some very interesting and mostly unusual steps determined by the nature of the metal centers.

(ii) The first step of the oxidation process corresponds to the oxidative addition of the I_2 molecule to one of the four-coordinated M(II) metal centers, aligned perpendicularly to the coordination plane, thus yielding a five-coordinated intermediate with square pyramidal stereochemistry. In this intermediate the favorable $n(M) \rightarrow \sigma^*_{I-I}$ MO orbital interactions support the transfer of the nonbonding electron pair belonging to the M(II) metal center to the antibonding σ^*_{I-I} MO, leading to a two-electron oxidation of the metal center and the concomitant rupture of the I−I bond. The electron transfer in a vacuum proceeds uphill on the potential energy surface (PES), without an intervening transition state.

(iii) The oxidized iodo complex $[(I)L_2M(\mu\text{-}PH_2)_2M'L_2]^-$ (L = CN) easily converts to a more stable intermediate involving a planar dimetallacycle five-membered ring, which through a reactant-like transition state with a relatively low barrier (18.5, 8.7, and 8.9 kcal/mol for Pt_2, PtPd, and Pd_2 compounds, respectively) yields the final product. At this reaction stage an unusual intramolecular reductive coupling of one of the ancillary ligands L with a bridging phosphido ligand takes place, resulting in the formation of a "Pt(II)(μ-PH_2)(μ-I)Pt(II)" framework. This step corresponds to an exoergic process by 11.4, 18.2, and 18.8 kcal/mol for Pt_2, PtPd, and Pd_2 compounds, respectively.

(iv) In the case of the Pt_2 and PtPd complexes removal of the iodide ligand from the oxidized intermediates $[(I)L_2M(\mu\text{-}PH_2)_2M'L_2]^-$ yields the very unusual $[L_2M^{III}(\mu\text{-}PH_2)_2M'^{III}L_2]$ (L = CN or C_6F_5) complexes displaying the metal centers in square planar coordination environments involving coplanar Pt(III)−Pt(III) and Pt(III)−Pd(III) bonds, respectively. The pentafluorophenyl Pt(III)−Pt(III) derivative was isolated, although we were not able to isolate the analogous Pt(III)−Pd(III) compound.

(v) In contrast, the analogous $[L_2Pd^{III}(\mu\text{-}PH_2)_2Pd^{III}L_2]$ compounds could not be identified as local minima in the PES, and it was impossible to isolate experimentally, as well. Instead, the equilibrium structure resulting from the intramolecular reductive coupling promoted by the iodide ligand abstraction corresponds to $[L_2Pd^{II}(\mu\text{-}PH_2)Pd^{II}(PH_2L)L]$ species, with the Pd(II) metal centers bridged by only one phosphido ligand. The $[(C_6F_5)_2Pd^{III}(\mu\text{-}PPh_2)_2Pd^{III}(C_6F_5)_2]$ complex was also impossible to isolate experimentally.

(vi) The $[L_2Pt^{II}(\mu\text{-}PH_2)Pt^{II}(PH_2L)L]$ species could be considered as intermediates for the reverse intramolecular oxidative addition of the PH_2L ligand promoted by iodide abstraction with Ag^+ ions.

(vii) Finally, the molecular structure of the $[(C_6F_5)_2Pd(\mu\text{-}PPh_2)(\mu\text{-}I)Pd(C_6F_5)\{PPh_2(C_6F_5)\}]$ complex has been established by X-ray crystallography and compared with the optimized structure at the B3LYP/LANL2DZ level of theory.

Experimental Section

General Data. C, H, and N analyses were performed with a Perkin-Elmer 240B microanalizer. IR spectra were recorded on a Perkin-Elmer Spectrum One spectrophotometer (Nujol mulls between polyethylene plates in the range 4000−350 cm^{-1}). NMR spectra were recorded on a Varian Unity 300 instrument with $SiMe_4$, $CFCl_3$, and 85% H_3PO_4 as external references for ^1H, ^{19}F, and ^{31}P, respectively. Conductivities (acetone, $c \approx 5 \times 10^{-4}$ M) were measured with a Philips PW 9509 conductimeter. Mass spectra were recorded on a VG-Autospec spectrometer operating at 30 kV, using the standard Cs-ion FAB gun and 3-nitrobenzyl alcohol as the matrix. Literature methods were used to prepare the starting complexes $[NBu_4]_2[(C_6F_5)_2M(\mu\text{-}PPh_2)_2M'(C_6F_5)_2]$ (M = M′ = Pt, **1a**; M = M′ = Pd, **1b**; M = Pt, M′ = Pd, **1c**).[46]

Reaction of $[NBu_4]_2[(C_6F_5)_2Pt(\mu\text{-}PPh_2)_2Pt(C_6F_5)_2]$ with I_2. (a) A CH_2Cl_2 (5 mL) solution of I_2 (0.013 g, 0.052 mmol) was added dropwise to a colorless solution of **1a** (0.100 g, 0.052 mmol) in CH_2Cl_2 (20 mL) at −78 °C. The solution quickly turned yellow, and after 10 min the solvent was evaporated to ca. 1.5 mL. A yellow solid began to crystallize and was left in the freezer for 5 h. The solid was filtered off and washed with cold CH_2Cl_2 (2 × 0.5 mL), forming **2** (0.056 g, 75%).

(b) A CH_2Cl_2 (5 mL) solution of I_2 (0.039 g, 0.156 mmol) was added dropwise to a colorless CH_2Cl_2 (25 mL) solution of **1a** (0.300 g, 0.156 mmol) at room temperature. The color of the solution quickly turned to yellow and after 20 h stirring (room temperature) fades to colorless. The solution was evaporated to ca. 1 mL, ^{i}PrOH (10 mL) was added, and by stirring a white solid crystallized, which was filtered off, washed with ^{i}PrOH (2 × 0.5 mL), and vacuum-dried. **3a**: 0.200 g, 71%. Anal. Found (calcd for $C_{64}F_{20}H_{56}INP_2Pt_2$): C, 42.7 (42.35); H, 3.1 (2.9); N, 0.8 (0.7). IR (X-sensitive[47,48] C_6F_5, cm^{-1}): 798 (s) and 776 (m). Λ_M = 66 Ω^{-1} cm^2 mol^{-1}. FAB-MS: *m*/*z* 1557 $[M]^-$, 1204 $[M - (PPh_2C_6F_5)]^-$. ^{19}F NMR (deuteroacetone, 293 K), δ: −114.2 (2 *o*-F, $J_{Pt,F}$ = 327 Hz), −115.0 (2 *o*-F, $J_{Pt,F}$ = 536 Hz), −115.4 (2 *o*-F, $J_{Pt,F}$ = 434 Hz), −124.5 (2 *o*-F, $PPh_2C_6F_5$), −152.0 (1 *p*-F, $PPh_2C_6F_5$), −162.9 (2 *m*-F, $PPh_2C_6F_5$), −165.4 (1 *p*-F) −165.6 (1 *p*-F), −165.7 (2 *m*-F), −166.1 (2 *m*-F), −167.3 (2 *m*-F), −167.4 (1 *p*-F) ppm. $^{31}P\{^1H\}$ NMR (deuteroacetone, 293 K, AX spin system, δ): 15.0 ($PPh_2C_6F_5$ $J_{Pt,P}$ = 2226 Hz), −55.3 (PPh_2 $J_{Pt,P}$ = 1981 and 1846 Hz) ppm. $^2J_{P,P}$ = 328 Hz.

Preparation of $[NBu_4][(C_6F_5)_2Pd(\mu\text{-}PPh_2)(\mu\text{-}I)Pd(C_6F_5)(PPh_2C_6F_5)]$ (3b). A CH_2Cl_2 (10 mL) solution of I_2 (0.030 g, 0.118 mmol) was added to a yellow CH_2Cl_2 (15 mL) solution

(44) Moncarz, J. R.; Brunker, T. J.; Glueck, D. S.; Sommer, R. D.; Rheingold, A. L. *J. Am. Chem. Soc.* **2003**, *125*, 1180−1181.
(45) Moncarz, J. R.; Laritcheva, N. F.; Glueck, D. S. *J. Am. Chem. Soc.* **2002**, *124*, 13356−13357.
(46) Forniés, J.; Fortuño, C.; Navarro, R.; Martínez, F.; Welch, A. J. *J. Organomet. Chem.* **1990**, *394*, 643−658.
(47) Maslowsky, E. J. *Vibrational Spectra of Organometallic Compounds*; Wiley: New York, 1997.
(48) Usón, R.; Forniés, J. *J. Adv. Organomet. Chem.* **1988**, *28*, 219−297.

Downloaded by NAT LIB UKRAINE on July 4, 2009
Published on March 18, 2004 on http://pubs.acs.org | doi: 10.1021/om034236y

of **1b** (0.200 g, 0.0115 mmol) and stirred at room temperature for 1.5 h. The solvent was evaporated almost to dryness, $CHCl_3$ (4 mL) was added, and the solution was concentrated to ca. 3 mL and left in the freezer overnight. A small amount of starting material (0.009 g) was crystallized and was filtered off. ^{i}PrOH (10 mL) was added to the filtrate, and the solution was evaporated to 8 mL. The mixture was stirred for 3 h and left in the freezer overnight. A yellow solid, **3b**, crystallized and was isolated by filtration, washed with ^{i}PrOH (2 × 0.5 mL), and vacuum-dried (0.105 g, 56%). Anal. Found (calcd for $C_{64}F_{20}H_{56}INP_2Pd_2$): C, 47.0 (47.4); H, 3.45 (3.5); N, 0.9 (0.9). IR (X-sensitive C_6F_5, cm^{-1}): 785 (s) and 761 (m). Λ_M = 114 Ω^{-1} cm^2 mol^{-1}. FAB-MS: *m*/*z* 1027 ([M − ($PPh_2C_6F_5$)]$^-$). ^{19}F NMR (deuteroacetone, 293 K), *δ*: −110.8 (2 *o*-F), −111.2 (2 *o*-F), −112.5 (2 *o*-F), −124.3 (2 *o*-F, $PPh_2C_6F_5$), −151.9 (1 *p*-F, $PPh_2C_6F_5$), −162.5 (2 *m*-F, $PPh_2C_6F_5$), −163.8 (1 *p*-F), −164.0 (2 *m*-F), −164.5 (1 *p*-F), −165.3 (3 *m* + *p*-F), −165.8 (2 *m*-F) ppm. ^{31}P{^{1}H} NMR (deuteroacetone, 293 K, AB spin system, *δ*): 9.6 (*P*$PPh_2C_6F_5$), 3.9 (*P*PPh_2) ppm. $^2J_{P,P}$ = 316 Hz.

Preparation of [NBu_4][(C_6F_5)$_2$Pt(*μ*-PPh_2)(*μ*-I)Pd(C_6F_5)($PPh_2C_6F_5$)] (3c). Complex **3c** (yellow solid) was prepared similarly to **3a** from **1c** (0.140 g, 0.077 mmol) and I_2 (0.020 g, 0.079 mmol) and 5 h stirring. **3c**: 0.038 g, 28%. Anal. Found (calcd for $C_{64}F_{20}H_{56}INP_2PdPt$): C, 44.5 (44.95); H, 3.2 (3.3); N 0.85 (0.8). IR (X-sensitive C_6F_5, cm^{-1}): 801 (s), 785 (m), and 773 (m). Λ_M = 112 Ω^{-1} cm^2 mol^{-1}. FAB-MS: *m*/*z* 1115 ([M − ($PPh_2C_6F_5$)]$^-$). ^{19}F NMR (deuteroacetone, 293 K), *δ*: −112.2 (2 *o*-F), −114.2 (2 *o*-F, $J_{Pt,F}$ = 337 Hz), −115.1 (2 *o*-F, $J_{Pt,F}$ = 533 Hz), −124.4 (2 *o*-F, $PPh_2C_6F_5$), −152.0 (1 *p*-F, $PPh_2C_6F_5$), −162.5 (2 *m*-F, $PPh_2C_6F_5$), −163.9 (1 *p*-F), −164.0 (2 *m*-F), −165.5 (1 *p*-F), −166.2 (2 *m*-F), −167.2 (3 *m* + *p*-F) ppm. ^{31}P-{^{1}H} NMR (deuteroacetone, 293 K, AX spin system, *δ*): 11.8 (*P*$PPh_2C_6F_5$), −18.7 (*P*PPh_2, $J_{Pt,P}$ = 1933 Hz) ppm. $^2J_{P,P}$ = 325 Hz.

Reaction of 3a with $AgClO_4$. $AgClO_4$ (0.030 g, 0.145 mmol) was added to a colorless CH_2Cl_2 (15 mL) solution of **3a** (0.150 g, 0.083 mmol), and the mixture was stirred in the dark for 5 h. After filtration the yellow solution was evaporated to dryness, and Et_2O (15 mL) was added. A white solid was filtered off (NBu_4ClO_4) and the solution evaporated to ca. 1 mL. Hexane (8 mL) was added, the solution evaporated to ca. 5 mL, and a yellow solid crystallized. This was identified (^{19}F and ^{31}P NMR spectroscopy) as **2**, 73%.

Crystal Structure Analysis of [NBu_4][(C_6F_5)$_2$Pd(*μ*-PPh_2)(*μ*-I)Pd(C_6F_5)($PPh_2C_6F_5$)] (3b). Crystal data and other details of the structure analysis are presented in Table 2. Suitable crystals of **3b** were obtained by slow diffusion of *n*-hexane into a solution of 0.020 g of [NBu_4][(C_6F_5)$_2$Pd(*μ*-PPh_2)(*μ*-I)Pd(C_6F_5)($PPh_2C_6F_5$)] in acetone (3 mL), and one of them was mounted at the end of a quartz fiber. Unit cell dimensions were initially determined from the positions of 256 reflections in 60 intensity frames measured at 0.3° intervals in *ω* and subsequently refined on the basis of positions of 5125 reflections from the main dataset. A hemisphere of data was collected based on three *ω*-scans runs (starting *ω* = −28°) at values *φ* = 0, 90, and 180 with the detector at 2*θ* = 28°. At each of these runs, frames (606, 435, and 230, respectively) were collected at 0.3° intervals and 10 s per frame. The diffraction frames were integrated using the SAINT package and corrected for absorption with SADABS.

The structure was solved by Patterson and Fourier methods. All refinements were carried out using the program SHELXL-97.[49] All non-hydrogen atoms were assigned anisotropic displacement parameters and refined without positional constraints. All hydrogen atoms were constrained to idealized geometries and assigned isotropic displacement parameters of 1.2 times the U_{iso} value of the attached carbon atoms (1.5 times for methyl hydrogen atoms). For the NBu_4^+ cation, the C atoms of two *n*-butyl chains were refined with a common set of anisotropic parameters each. The C−C distance between one of the methyl C atoms and the one adjacent was constrained to a sensible value. Full-matrix least-squares refinement of this model against F^2 converged to final residual indices given in the Supporting Information (Table S1). The final difference electron density map showed one feature above 1 e/Å^3 (max./min. 1.13/−1.35 e/Å^3) located at 0.95 Å from the iodine atom.

Table 2. Crystal Data and Structure Refinement for [NBu_4][(C_6F_5)$_2$Pd(*μ*-PPh_2)(*μ*-I)Pd(C_6F_5)($PPh_2C_6F_5$)] (3b)

empirical formula	$C_{64}H_{56}F_{20}INP_2Pd_2$
unit cell dimensions	
a (Å)	11.9793(9)
b (Å)	13.6815(10)
c (Å)	22.1965(16)
α (deg)	101.270(1)
β (deg)	99.102(1)
γ (deg)	107.689(2)
volume (Å^3), *Z*	3305.6(4), 2
wavelength (Å)	0.71073
temperature (K)	293(1)
radiation	graphite monochromated Mo Kα
space group	$P\bar{1}$
cryst dimens (mm)	0.45 × 0.25 × 0.15
abs coeff (mm^{-1})	1.155
transmission factors	1.000, 0.621
diffractometer	Bruker Smart Apex
2*θ* range for data collection (deg)	3.2 to 49.6 (±*h*, ±*k*, ±*l*)
no. of reflns collected	17 682
no. of indep reflns	11 057 [*R*(int) = 0.0820]
goodness-of-fit on F^2 [a]	1.037
final *R* indices [$I > 2\sigma(I)$] [b]	R1 = 0.0721, wR2 = 0.1754
R indices (all data)	R1 = 0.1025, wR2 = 0.2006

[a] Goodness-of-fit = $[\sum w(F_o^2 - F_c^2)^2/N_{obs} - N_{param}]^{0.5}$. [b] R1 = $\sum||F_o| - |F_c||/\sum|F_o|$; wR2 = $[\sum w(F_o^2 - F_c^2)^2/\sum wF_o^4]^{0.5}$.

Computational Methods

All the calculations were performed using the GAUSSIAN 98 program package.[50] The equilibrium and transition structures were fully optimized by Becke's three-parameter hybrid functional[51,52] combined with the Lee−Yang−Parr[53] correlation functional abbreviated as B3LYP level of density functional theory, using the LANL2DZ basis set. Control calculations were also carried out using the LANL2DZ basis set for the metal and iodine atoms and 6-31G(d,p) for the rest of the non-metal atoms. Full geometry optimization was performed for each structure using Schlegel's analytical gradient method,[54] and the attainment of the energy minimum was verified by calculating the vibrational frequencies that result in the absence of imaginary eigenvalues. All the stationary points have been identified for minima (number of imaginary frequencies NIMAG = 0) or transition states (NIMAG = 1). The computed electronic energies, the enthalpies of reactions,

(49) Sheldrick, G. M. *SHELXL-97* a program for crystal structure determination; University of Gottingen: Germany, 1997.

(50) Frisch, M. J.; T., G. W.; Schlegel, H. B.; Scusseria, G. E.; Robb, M. A.; Cheeseman, J. R.; Zakrzewski, V. G.; Montgomery, J. A.; Stratmann, R. E.; Burant, J. C.; Dapprich, S.; Millan, J. M.; Daniels, A. D.; Kudin, K. N.; Strain, M. C.; Farkas, O.; Tomasi, J.; Barone, V.; Cossi, M.; Cammi, R.; Mennucci, B.; Pomelli, C.; Adamo, C.; Clifford, S.; Orchterski, J.; Petersson, G. A.; Ayala, P. Y.; Cui, Q.; Morokuma, K.; Malick, D K.; Rabuck, A. D.; Raghavachari, K.; Foresman, J. B.; Cioslowski, J.; Ortiz, J. V.; Stefanov, B. B.; Liu, G.; Liashenko, A.; Piskorz, P.; Komaroni, I.; Gomperts, R.; Martin, R. L.; Fox, D. J.; Keith, T.; Al-Laham, M. A.; Peng, C. Y.; Nanayakkara, A.; Gonzalez, C.; Challacombe, M.; Gill, P. M.; Johnson, P.; Chen, W.; Wong, M. W.; Andres, J. L.; Head-Gordon, M.; Replogle, E. S. *Gaussian 98*, Revision A.7; Gaussian Inc.: Pittsburgh, PA, 1998.

(51) Becke, A. D. *J. Chem. Phys.* **1992**, *96*, 215.

(52) Becke, A. D. *J. Chem. Phys.* **1993**, *98*, 5648.

(53) Lee, C.; Yang, W.; Parr, R. G. *Phys. Rev.* **1998**, *B 37*, 785.

(54) Schlegel, H. B. *J. Comput. Chem.* **1982**, *3*, 214.

$\Delta_R H_{298}$, and the activation energies, $\Delta G^{\ddagger}_{298}$, were corrected to constant pressure and 298 K, for zero-point energy (ZPE) differences, and for the contributions of the translational, rotational, and vibrational partition functions. For transition state geometry determination, quasi-Newton transit-guided (QSTN) computations were performed.[55] Moreover, intrinsic reaction paths (IRPs)[56,57] were traced from the various transition structures to make sure that no further intermediates exist.

Because of the computational cost due to the relatively big size of the compounds under consideration, to obtain a computationally convenient size, we used models resulting upon substitution of the phenyl groups of the phosphido ligands by H atoms, while the C_6F_5 group was replaced by the CN group. The choice of substitution of the C_6F_5 ligands by the CN ones was based on electronic structure calculations at the B3LYP/6-31G(d,p) level of the coordinating ability (σ-donor and π-acceptor capacity) of the ligands by examining the nature and energy of their frontier molecular orbitals (FMOs). The two ligands exhibit the same pattern of FMOs, consisting of a highest occupied molecular orbital (HOMO), corresponding to a hybridized orbital localized mainly on the C donor atom, and a lowest unocuppied molecular orbital (LUMO) corresponding to a π^* MO delocalized over the entire nuclear framework. We also performed calculations on model complexes resulting upon substitution of the C_6F_5 ligands by the CF_3 ones. From an electronic point of view, the CF_3 ligand differs remarkably from the C_6F_5 one, since the former is a weak pure σ-donor ligand. Comparison of the computed geometrical parameters of the $[(C_6F_5)_2Pt(\mu\text{-}PH_2)_2Pt(C_6F_5)_2]$, $[(CN)_2Pt(\mu\text{-}PH_2)_2Pt(CN)_2]$, and $[(CF_3)_2Pt(\mu\text{-}PH_2)_2Pt(CF_3)_2]$ complexes strongly justifies our choice to substitute the C_6F_5 by the CN ligands. Thus, R_e(Pt−Pt) = 2.875, 2.844, and 2.980 Å; R_e(Pt−P) = 2.388, 2.403, and 2.433 Å; θ_e(P−Pt−P) = 106.0°, 106.4°, and 105.3°; θ_e(Pt−P−Pt) = 74.0°, 73.6°, and 75.5° for the C_6F_5, CN, and CF_3 derivatives, respectively. Moreover, the coordination environment of the two platinum centers in the $[(CF_3)_2Pt(\mu\text{-}PH_2)_2Pt(CF_3)_2]$ model is not square planar; the C−P−P−C dihedral angle is 31.5°.

The use of such models does not alter the description of the "core" region of the compounds and is ultimately the most efficient and productive route to modeling the electronic structure and related properties of relatively big-sized transition metal coordination compounds.

Although substituents on the bridging phosphido groups are expected to remotely tune the electronic structure of the complexes, their effects on the structures of the complexes would be comparable along the series. This is substantiated through the comparison of the computed geometrical parameters of the $[(C_6F_5)_2Pt(\mu\text{-}PH_2)_2Pt(C_6F_5)_2]$ complex reported previously[3] to those of the real $[(C_6F_5)_2Pt(\mu\text{-}PPh_2)_2Pt(C_6F_5)_2]$ complex determined experimentally.

Acknowledgment. We thank the Ministerio de Ciencia y Tecnología y Fondos FEDER for its financial support (Project BQU2002-03997-CO2-02) and the Agencia Española de Cooperación Internacional (Ministerio de Asuntos Exteriores) for a grant to N.Ch.

Supporting Information Available: Tables of full atomic positional and equivalent isotropic displacement parameters, anisotropic displacement parameters, full bond distances and bond angles, and hydrogen coordinates and anisotropic displacement parameters for the crystal structure of complex **3b**. Figures S1−S6 showing the equilibrium geometries of all species involved in the oxidative addition and intramolecular reductive coupling reactions. Table S1 summarizing the Cartesian coordinates and energies of all stationary points (PDF). This information is available free of charge via the Internet at http://pubs.acs.org.

OM034236Y

(55) Head-Gordon, M.; P., J. A.; Frisch, M. *Chem. Phys. Lett.* **1988**, *153*, 503.
(56) Gonzalez, C.; Schlegel, H. B. *J. Chem. Phys.* **1989**, *90*, 2154.
(57) Gonzalez, C.; Schlegel, H. B. *J. Phys. Chem.* **1990**, *94*, 5523.
(58) Alonso, E.; Forniés, J.; Fortuño, C.; Martín, A.; Orpen, A. G. *Organometallics* **2003**, *22*, 5011−5019.

Downloaded by NAT LIB UKRAINE on July 4, 2009
Published on March 18, 2004 on http://pubs.acs.org | doi: 10.1021/om034236y